Engineering Letters

Effect of Ambient Temperature and Intake Humidity on the Cold Start Performance of PEMFC

Hongyan Wang, Qian Hong, Binbin Sun, Pengwei Wang, Bintao Li

***Abstract*—To address the cold start problem of proton exchange membrane fuel cell, this paper investigates the influence of ambient temperature and cathode inlet relative humidity on the cold start performance of PEMFC. First, a mathematical model of PEMFC cold start was established, and then a three-dimensional, dynamic, multi-parameter, and multi-physical field coupling simulation model was designed for the analysis of PEMFC cold start performance based on COMSOL software platform. Based on the model, the effects of ambient temperature and cathode inlet relative humidity on the characteristics of PEMFC, such as current density, temperature change and icing condition are analyzed during the cold start process. In this study, only the PEMFC at -7 °C successfully self-started, while the PEMFCs at -20 °C and -10 °C failed due to severe icing and performance deterioration. The results show that a higher ambient temperature helps to stabilize the output performance of the cold start process, delays icing, and prolongs the survival time under cold start conditions. In the -10 °C environment, the PEMFC failed to achieve a cold start under all three cathode inlet relative humidity conditions of 0%, 30%, and 60%, indicating that the cathode humidification has a very limited improvement on the fuel cell power and heat production performance, while increasing the risk of ice accumulation.**

***Index Terms*—PEMFC, cold start, ambient temperature, intake humidity, influence mechanism**

I. INTRODUCTION

PROTON exchange membrane fuel cell (PEMFC) is considered as one of the most promising future power sources for automobiles due to the advantages of cleaner products and higher energy density. Cold start is a dynamic process in which a fuel cell is started from sub-zero temperatures and operated until it reaches its normal operating temperature. The key to a successful cold start lies in utilizing the heat generated by the electrochemical reaction to raise the temperature of the electric stack above the freezing point before the cathode catalytic layer (CCL) is completely covered by ice [1,2]. However, during cold start at low temperatures, the electrochemical reaction product water accumulates and freezes in the structural pores of the catalytic layer (CL) and the gas diffusion layer (GDL) to block the gas flow channels, hindering the electrochemical reaction, leading to the failure of the fuel cell to start and causing structural damage to the membrane electrode assembly (MEA) [3,4].

Many experts and scholars have focused their studies on the influencing factors of fuel cell cold starts, particularly on structural parameters and starting conditions. Santamaria A.D. [5] investigated the effect of flow field structure on the cold start performance of PEMFCs and found that the cross-finger flow field enhanced the forced convection of reactive gas into the porous electrodes compared to the parallel flow field, improving the water removal capability under the ribs. Luo [6] established a cold start model for multiphase power stacks and found that the greater the number of monolithic cells, the faster the temperature rise. Balliet [7] simulated the transport of liquid water, water vapor, and ice formation, and found that increasing the ionomer volume fraction in the catalytic layer (CL) could reduce the cold start time. Yang [8] and Zang [9] investigated the effect of CL parameters on the cold start performance of PEMFCs and found that the competition between the loss of reactant concentration in agglomerates and the active electrocatalytic surfaces leads to different cold start failure modes.

On the other hand, Jiang [10] investigated the effect of initial current density on the cold start performance of fuel cells and found that increasing the initial current density can accelerate the rate of heat generation and raise the cell temperature. However, the amount of water produced and accumulated in the cathode catalytic layer (CCL) also increases more rapidly, leading to faster ice formation and ultimately causing cold start failure. Pinton [11] conducted isothermal constant potential and constant current tests on a single cell under multiple operating conditions in a sub-zero temperature environment. They found that ice formation at the active reaction sites of the CCL, even at the optimal wetting level of the cell, hinders oxygen transport and

Manuscript received February 19, 2025; revised April 17, 2025.

This work was supported in part by the Postdoctoral Science Foundation of Shandong under Grant ZR2024ME179, the Innovation team project of "Qing-Chuang science and technology plan" of colleges and universities in Shandong Province 2021K1083, Major Innovation Projects in Shandong under Grant 2020CXGC010405 and 2020CXGC010406.

Hongyan Wang is a graduate student of School of Transportation and Vehicle Engineering, Shandong University of Technology, Zibo, 255000 PR China. (e-mail: 19811730129@163.com)

Qian Hong is a Lecturer of School of Mechanical and Electrical Engineering, Shandong Vocational College of Industry, Zibo 256414 PR China. (e-mail: 377762483@qq.com).

Binbin Sun is a Professor of School of Transportation and Vehicle Engineering, Shandong University of Technology, Zibo, 255000 PR China. (corresponding author to provide phone: 86-13708941464; e-mail: Sunbin_sdut@126.com).

Pengwei Wang is a Professor of School of Transportation and Vehicle Engineering, Shandong University of Technology, Zibo, 255000 PR China. (corresponding author to provide phone: 86- 13287825788; e-mail: wpwk16@163.com).

Bintao Li is a graduate student of School of Transportation and Vehicle Engineering, Shandong University of Technology, Zibo, 255000 PR China. (e-mail: 13968154214@163.com)

increases cell resistance, significantly reducing the cell's performance under load. Tao [12] found that cold starting by controlling the voltage can accelerate the temperature rise of the PEMFC, which is conducive to successful cold starts.

This paper is based on a three-dimensional transient multi-physics model of a PEMFC developed in COMSOL. It investigates the effects of ambient temperature and cathode inlet relative humidity on the cold start process. The analysis reveals the changes in the output performance, temperature variations, and freezing conditions of the PEMFC under different operating conditions, providing guidance for the adjustment of cold start parameters and strategy optimization.

II. PEMFC COLD START MODELLING

A. Model Assumptions

The PEMFC cold start simulation is complex, involves a variety of physical phenomena, and faces problems such as strong nonlinearity and poor convergence when using COMSOL software. Therefore, reasonable assumptions need to be made about the model to achieve fast and effective simulation. The following are the basic assumptions of the model:

(1) Gases such as hydrogen and oxygen cannot penetrate the Proton exchange membrane (PEM);

(2) The reaction gases are all ideal gases;

(3) The internal gases are all incompressible laminar flow;

(4) PEM, CL, and GDL are homogeneous porous media structures with isotropy;

(5) The structural deformation and gravity factors inside the cell are ignored;

(6) The inlet air is not humidified, and any water inside the flow channels is immediately removed;

(7) The electrochemical double-layer charging and discharging characteristics in CL are negligible.

B. PEMFC Model Control Equations

The fuel cell cold start model is primarily solved based on the equations of charge conservation, mass conservation, momentum conservation, energy conservation, and component conservation.

Generally, the transport processes of hydrogen ions and electrons in a fuel cell are described by the following equations for the conservation of ion potential and electron potential:

$$0=\nabla\cdot(\kappa_{ion}^{eff}\nabla\varphi_{ion})+S_{ion} \tag{1}$$

$$0=\nabla\cdot(\kappa_{e}^{eff}\nabla\varphi_{e})+S_{e} \tag{2}$$

where, κ_{ion}^{eff} , $\kappa_{\mathrm{e}}^{\mathrm{eff}}$ are the effective ionic conductivity and effective electronic conductivity, respectively ($\mathrm{s\cdot m^{-1}}$), φ_{ion} is the ionic potential in the electrolyte, φ_{e} is the electron potential at the porous electrode and the polar plate ($\mathrm{s\cdot m^{-1}}$), S_{ion} , S_{e} are the ion source term and the electron source term, respectively ($\mathrm{A\cdot m^{-3}}$).

The mass conservation equation for a mixture of hydrogen, oxygen, and water vapor is:

$$\frac{\partial}{\partial t}\left(\varepsilon\left(1-s_{\mathrm{lq}}-s_{\mathrm{ice}}\right)\rho_{\mathrm{g}}\right)+\nabla\cdot\left(\rho_{\mathrm{g}}\vec{u}_{\mathrm{g}}\right)=S_{\mathrm{m}} \tag{3}$$

where, ε is the porosity of CL and GDL, ρ_{g} is the gas mixture density ($\mathrm{kg\cdot m^{-3}}$), s_{lq} , s_{ice} are the liquid water volume fraction and ice volume fraction, respectively, $\vec{u}_{\mathrm{g}}$ is the gas flow rate ($\mathrm{m\cdot s^{-1}}$), and S_{m} is the gas mixture mass source term ($\mathrm{kg\cdot m^{-3}\cdot s^{-1}}$), which is equal to the sum of the hydrogen and oxygen mass source terms and the water vapor mass source term.

The equation for the conservation of mass of water in the membrane state is:

$$\frac{\rho_{\mathrm{mem}}}{\mathrm{EW}}\frac{\partial}{\partial t}\left(\omega\lambda_{\mathrm{nf}}\right)=\frac{\rho_{\mathrm{mem}}}{\mathrm{EW}}\nabla\cdot\left(D_{\mathrm{mw}}^{\mathrm{eff}}\nabla\lambda_{\mathrm{nf}}\right)+S_{\mathrm{nfm}} \tag{4}$$

The left side of the equation is the transient term, and the right side of the equation is the diffusion and mass source terms, respectively. ρ_{mem} is the dry state density of PEM ($\mathrm{g\cdot m^{-3}}$), EW is the equivalent mass of PEM ($\mathrm{g\cdot mol^{-3}}$), λ_{nf} is the water content of the membrane in the non-frozen membrane state, ω is the volume fraction of the CL ionomer, $D_{\mathrm{mw}}^{\mathrm{eff}}$ is the effective diffusion coefficient of the water in the non-frozen membrane state ($\mathrm{m^{2}\cdot s^{-1}}$), and S_{nfm} is the source of the mass term of the water in the non-frozen membrane state ($\mathrm{kg\cdot m^{-3}\cdot s^{-1}}$).

The mass conservation equation for membrane ice (frozen membrane water) is:

$$\frac{\rho_{mem}}{EW}\frac{\partial(\omega\lambda_{f})}{\partial t}=S_{fmw} \tag{5}$$

where, λ_{f} represents the content of frozen membrane water, and S_{fmw} represents the mass source term of the frozen membrane water.

The equation for conservation of mass for liquid water is:

$$\frac{\partial}{\partial t}\left(\rho_{\mathrm{lq}}\varepsilon s_{\mathrm{lq}}\right)=\nabla\cdot\left(\rho_{\mathrm{lq}}D_{\mathrm{lq}}\nabla s_{\mathrm{lq}}\right)+S_{\mathrm{lq}} \tag{6}$$

ρ_{lq} is the density of liquid water ($\mathrm{kg\cdot m^{-3}}$), D_{lq} is the diffusion coefficient of liquid water ($\mathrm{m^{2}\cdot s^{-1}}$), S_{lq} and is the liquid water mass source term ($\mathrm{kg\cdot m^{-3}\cdot s^{-1}}$), which consists of two parts: the phase transition from water vapor to liquid water and the phase transition from liquid water to ice.

The mass conservation equation for ice is:

$$\frac{\partial}{\partial t}\left(\rho_{\mathrm{ice}}\varepsilon s_{\mathrm{ice}}\right)=S_{\mathrm{ice}} \tag{7}$$

Where, ρ_{ice} is the ice bulk density ($\mathrm{kg\cdot m^{-3}}$), s_{ice} is the ice volume fraction, S_{ice} is the ice mass source term, It consists of two components, the condensation icing source term from water vapor to ice and the solidification icing source term from liquid water to ice.

The gas-phase flow inside the PEMFC follows the momentum conservation equation:

$$\frac{\partial}{\partial t}\left(\frac{\rho_{\mathrm{g}}\vec{u}_{\mathrm{g}}}{\varepsilon\left(1-s_{\mathrm{lq}}-s_{\mathrm{ice}}\right)}\right)+\nabla\cdot\left(\frac{\rho_{\mathrm{g}}\vec{u}_{\mathrm{g}}\vec{u}_{\mathrm{g}}}{\varepsilon^{2}\left(1-s_{\mathrm{lq}}-s_{\mathrm{ice}}\right)^{2}}\right)=-\nabla p_{\mathrm{g}}$$
$$+\mu_{\mathrm{g}}\nabla\cdot\left(\nabla\left(\frac{\vec{u}_{\mathrm{g}}}{\varepsilon\left(1-s_{\mathrm{lq}}-s_{\mathrm{ice}}\right)}\right)+\nabla\left(\frac{\vec{u}_{\mathrm{g}}^{\,T}}{\varepsilon\left(1-s_{\mathrm{lq}}-s_{\mathrm{ice}}\right)}\right)\right) \quad (8)$$
$$-\frac{2}{3}\mu_{\mathrm{g}}\nabla\cdot\left(\nabla\left(\frac{\vec{u}_{\mathrm{g}}}{\varepsilon\left(1-s_{\mathrm{lq}}-s_{\mathrm{ice}}\right)}\right)\right)+S_{\mathrm{u}}$$

Where, p_{g} is the gas-phase pressure (Pa), μ_{g} is the gas-phase kinetic viscosity ($\mathrm{kg\cdot m^{-1}\cdot s^{-1}}$), and S_{u} is the momentum source term ($\mathrm{kg\cdot m^{-3}\cdot s^{-1}}$).

The energy conservation equation is:

$$\frac{\partial}{\partial t}\left(\left(\rho C_{\mathrm{p}}\right)_{\mathrm{fl,sl}}^{\mathrm{eff}}T\right)+\nabla\left(\left(\rho C_{\mathrm{p}}\right)_{\mathrm{fl}}^{\mathrm{eff}}\vec{u}_{\mathrm{g}}T\right)=\nabla\cdot\left(k_{\mathrm{fl,sl}}^{\mathrm{eff}}\nabla T\right)+S_{\mathrm{T}} \quad (9)$$

Where, the first term to the left of the equal sign is the transient term and the second term is the convective heat transfer term. $\left(\rho C_{\mathrm{p}}\right)_{\mathrm{fl,sl}}^{\mathrm{eff}}$ is the effective volumetric heat capacity ($\mathrm{J\cdot kg^{-1}\cdot K^{-1}}$), $k_{\mathrm{fl,sl}}^{\mathrm{eff}}$ is the effective thermal conductivity ($\mathrm{W\cdot m^{-1}\cdot K^{-1}}$), T is the temperature (K), and S_{T} is the energy source term, which mainly consists of the activation heat source term, the ohmic heat source term, the phase transition latent heat source term, and the electrochemical reversible heat source term.

The gas component conservation equation is:

$$\frac{\partial}{\partial t}\left(\varepsilon\left(1-s_{\mathrm{lq}}-s_{\mathrm{ice}}\right)\rho_{\mathrm{g}}Y_{i}\right)+\nabla\cdot\left(\rho_{\mathrm{g}}\vec{u}_{\mathrm{g}}Y_{i}\right)=\nabla\cdot\left(\rho_{\mathrm{g}}D_{i}^{\mathrm{eff}}\nabla Y_{i}\right)+S_{i} \quad (10)$$

Where, Yi is the mass fraction of gas i, which consists of hydrogen, oxygen, water vapor and nitrogen, D_{i}^{eff} is the effective diffusion coefficient of gas component i, and S_{i} is the mass source term of each gas component, which indicates the mass consumption of the gas component in the electrochemical reaction process.

C. PEMFC Three-Dimensional Multiphysics Field Models

In this paper, we simplify and construct a 3D geometric model of the fuel cell stack based on the physical structure of the PEMFC, as shown in Figure 1. The geometric dimensions of the single-channel PEMFC model are 3.47 mm × 2 mm × 20 mm. The inlet and outlet of the gas channel are squares with a length and height of 1 mm, and the width of the channel rib is 1 mm. The model consists of a 5-layer MEA structure and a bipolar plate (BP), with the main components of the stack labeled in the figure.

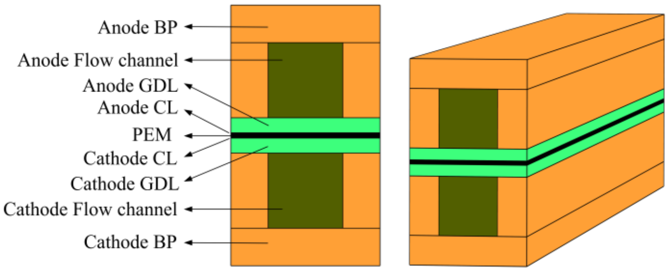

Fig. 1. Geometric model of PEMFC

Table 1 presents the geometric and physical parameters of the PEMFC stack model. It includes the specific geometric dimensions of the PEMFC and the values of parameters related to various physical fields, such as conductivity, thermal conductivity, heat capacity, permeability, porosity, and others.

TABLE I
GEOMETRIC AND PHYSICAL PARAMETERS OF PEMFC MODEL

Parameter	Value
Thickness of PEM, CL, GDL	0.127, 0.01, 0.2 mm
Membrane density of PEMFC	$1980\ \mathrm{kg\cdot m^{-3}}$
Membrane equivalent mass	$1100\ \mathrm{g\cdot mol^{-1}}$
Gas flow channel length, Width, height	20, 1, 1 mm
Porosity of CL, GDL	0.3, 0.6
Contact angle of CL, GDL	100°, 120°
Volume fraction of the ionomer in CL	0.25
Conductivity of CL, GDL, BP	$300, 300, 20000\ \mathrm{S\cdot m^{-1}}$
Heat conductivity of PEM, CL, GDL, BP	$0.95, 1, 1, 20\ \mathrm{W\cdot m^{-1}\cdot K^{-1}}$
Specific heat capacity of PEM, CL, GDL, BP	$833, 3300, 568, 1580\ \mathrm{J\cdot kg^{-1}\cdot K^{-1}}$
Intrinsic permeabilities of CL, GDL	$6.2\times10^{-13}, 6.2\times10^{-12}\ \mathrm{m^{2}}$
Starting voltage	0.7 V
Density of liquid water, ice	$990, 920\ \mathrm{kg\cdot m^{-3}}$
Specific heat capacity of hydrogen, oxygen, water vapor, liquid water, ice	$14283, 919, 2014, 4182, 2060\ \mathrm{J\cdot kg^{-1}\cdot K^{-1}}$
Rate of evaporation, condensation, melting, sublimation	$1\ \mathrm{s^{-1}}$

When establishing the cold start model of a fuel cell, the setting of boundary conditions significantly influences the model's output results. Reasonable boundary conditions ensure the accuracy of the model's predictions. The inlet boundary condition is defined as a mass flow rate, which is calculated based on the actual operating conditions of the fuel cell, while the outlet is set as a pressure boundary condition. The cathode and anode inlet mass flow rates are determined by the following equations [13,14].

$$\dot{m}_{\mathrm{a}}=\frac{S_{\mathrm{a}}\rho_{\mathrm{g}}^{\mathrm{a}}I_{\mathrm{ref}}A_{\mathrm{mem}}}{2Fc_{\mathrm{H_2}}},\ \dot{m}_{\mathrm{c}}=\frac{S_{\mathrm{c}}\rho_{\mathrm{g}}^{\mathrm{c}}I_{\mathrm{ref}}A_{\mathrm{mem}}}{4Fc_{\mathrm{O_2}}} \quad (11)$$

Where, S_{a}, S_{c} is the stoichiometric ratios of the anode and cathode gas supply, $\rho_{\mathrm{g}}^{\mathrm{a}}$, $\rho_{\mathrm{g}}^{\mathrm{c}}$ is the density of cathode and anode inlet gas mixture, I_{ref} is the reference current density, A_{mem} is the active reaction area, $c_{\mathrm{H_2}}$, $c_{\mathrm{O_2}}$ is the concentration of hydrogen at the anode side and oxygen at the cathode side, respectively, and F is the Faraday constant.

There is heat exchange between the surface of the fuel cell and the external environment. The thermal boundary conditions are determined by the heat transfer coefficient of the fuel cell surface. Therefore, the rate of heat transfer between the fuel cell and the external environment is given by:

$$\dot{Q} = hA_{\text{wall}}\left(T_{\text{surr}} - T_{\text{wall}}\right) \qquad (12)$$

Where h is the convective heat transfer coefficient of the surface, 50 $W \cdot m^{-2} \cdot K^{-1}$, A_{wall}, T_{wall} are the surface area and temperature of the external wall, T_{surr} is the external ambient temperature.

D. Model Validation

To verify the correctness of the fuel cell cold start model established above, the Nafion N115 (127 mm) membrane is selected for validation under two operating conditions: ambient temperature (15 °C) and low temperature (-5 °C). The polarization curves obtained from experiments and simulations are shown in Figure 2. Under both ambient temperatures, the measured values are in good agreement with the simulated values when the PEMFC operates in the low and medium current density ranges. However, in the high current density range, the output performance of the PEMFC simulated by the model deviates slightly from the measured values. This deviation is primarily due to the rapid production of water from the electrochemical reaction at high output currents, combined with the poor drainage performance of the multi-channel parallel flow field used in the experiments, which is prone to local flooding and ice accumulation due to the presence of multiple inlet and exhaust manifolds. Nevertheless, the resulting deviation is within 5%, confirming the structural feasibility of the constructed fuel cell simulation model.

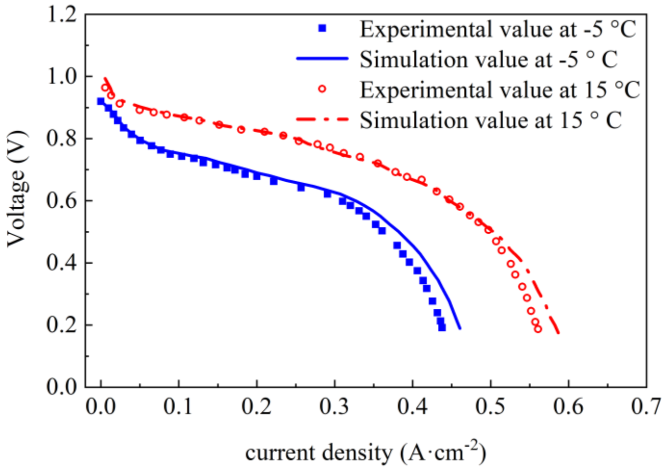

Fig. 2 Comparison of polarization curves between simulation and experiment

III. EFFECT OF AMBIENT TEMPERATURE ON COLD START PERFORMANCE OF PEMFC

A. Current Density During Cold Start at Different Starting Temperatures

In this section, three different ambient temperatures, -20 °C, -10 °C, and -7 °C are set as the basic cold start conditions for comparative study. Figure 3 depicts the variation of the output current density of the PEMFC under cold start conditions at these three temperatures. The results show that the cold start fails in both the -20 °C and -10 °C environments, with the current density initially rising and then rapidly decreasing, reflecting rapid internal ice accumulation. In contrast, the PEMFC cold start is successful in the -7 °C environment, with a steady rise in current density and the cell temperature increasing above the freezing point.

At -20 °C, the fuel cell fails to start within 60 seconds due to rapid ice accumulation. At -10 °C, the rising trend of current density lasts longer, which corresponds to the slower accumulation of ice in the CCL reaching a critical value. However, it ultimately fails after 240 seconds due to ice accumulation and insufficient temperature rise. At -7 °C, the internal icing phenomenon in the fuel cell is reduced, and the higher temperature leads to stronger electrochemical reaction kinetics, significantly increasing water and heat production. At this temperature, as the cell temperature rises, the saturated water content of the electrolyte increases synchronously, and the amount of product water undergoing ice phase transition is small. As a result, the average cell temperature steadily rises to the freezing point within 96 seconds, and the PEMFC successfully self-starts at -7 °C.

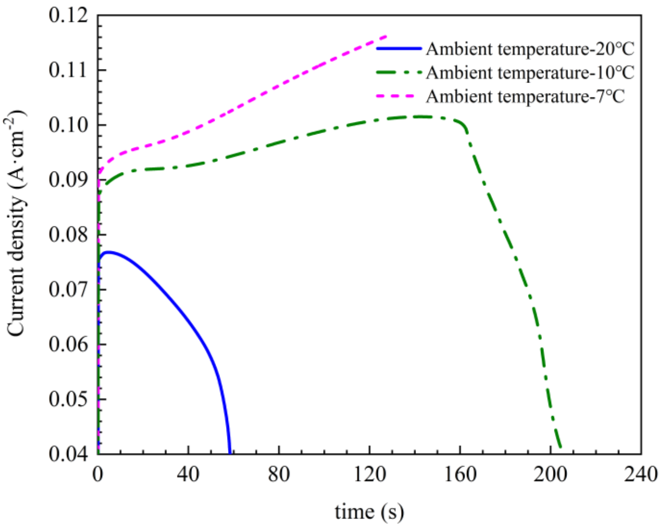

Fig. 3 Evolution of output current density of PEMFC during the cold start processes of different initial temperatures

B. Ice Volume Fraction During Cold Start Of PEMFC At Different Starting Temperatures

The CL icing of the PEMFC during the cold start process at three initial ambient temperatures is shown in Figure 4 below. At -20 °C, the ice accumulation phenomenon in the PEMFC CCL is the most severe, with the highest ice volume fraction and the fastest ice accumulation rate. The ice volume fraction exceeds 0.9 within 60 seconds, resulting in cold start failure. In contrast, in the -10 °C environment, there is no icing in the CCL during the first 15 seconds. However, after this period, the membrane water content in the local area of the membrane electrode reaches the critical saturation value, leading to ice accumulation. Nevertheless, the icing effect is weaker than that at -20 °C. In the -7 °C environment, the output performance of the PEMFC is the best, and the average ice volume fraction remains a horizontal straight line, indicating no significant icing in the CCL during the startup process. The output current density increases steadily, the electrochemical performance is excellent, and the self-start is successfully achieved within 120 seconds. Therefore, the initial ambient temperature is a critical factor affecting internal ice accumulation during the cold start stage of the PEMFC, and a higher ambient temperature can significantly delay and mitigate the ice accumulation effect.

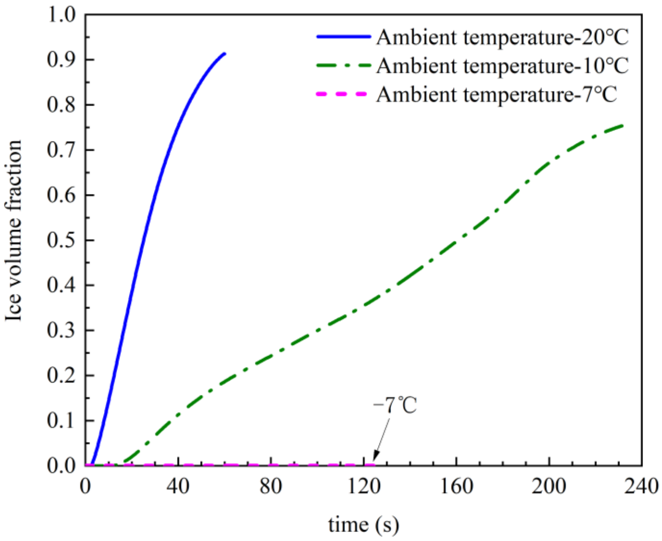

Fig. 4 Evolution of ice volume fraction in cathode CL during the cold start processes of different initial temperatures

Figure 5 shows the distribution of the CCL ice volume fraction over time during the cold start test at three initial ambient temperatures, with the inlet side of the supplied gas located at the left end of the contour. It can be observed that the -20 °C cold start scheme begins to freeze the earliest, followed by the -10 °C cold start scheme, while the -7 °C scheme exhibits very little ice formation throughout the entire startup stage. Ultimately, only the PEMFC in the -7 °C environmental scenario successfully self-starts among the three schemes, whereas the other two schemes fail due to severe icing and performance degradation.

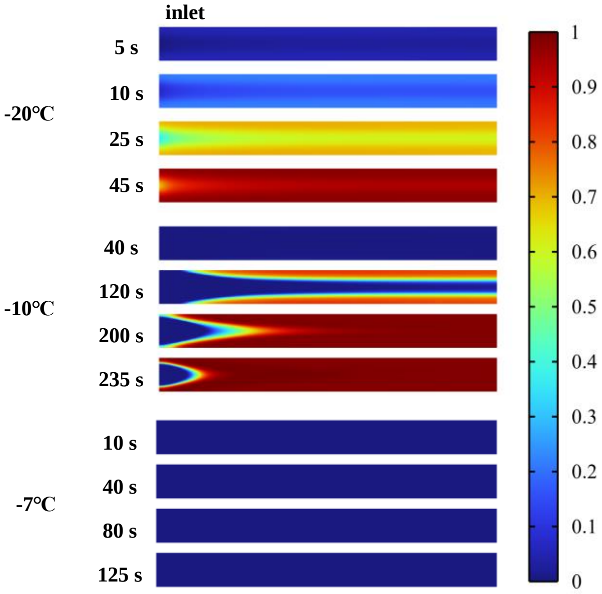

Fig. 5 Evolution of distribution of ice volume fraction in cathode CL during the cold start processes of different initial temperatures

C. *Temperature Changes During Cold Start Of PEMFC At Different Starting Temperatures*

Figure 6 compares the temperature changes of the PEMFC cold start at three different initial ambient temperatures. In the -20 °C and -10 °C startup schemes, the cell temperature initially rises and then levels off before decreasing. The maximum average temperatures reach -16 °C and -3 °C, respectively, but neither exceeds the freezing point. At the end, the temperature slightly decreases, resulting in cold start failure. In contrast, the average cell temperature at -7 °C continues to rise, exhibiting two stages: rapid warming followed by steady warming. It reaches the freezing point approximately 96 seconds after startup and continues to rise steadily. This result demonstrates the successful cold start of the PEMFC below freezing under this scheme, while also proving that PEMFCs possess certain low-temperature self-starting capability at relatively higher initial ambient temperatures. However, when the ambient temperature drops to more severe conditions such as -10 °C or -20 °C, conventional unassisted PEMFC cold starts become extremely difficult to achieve.

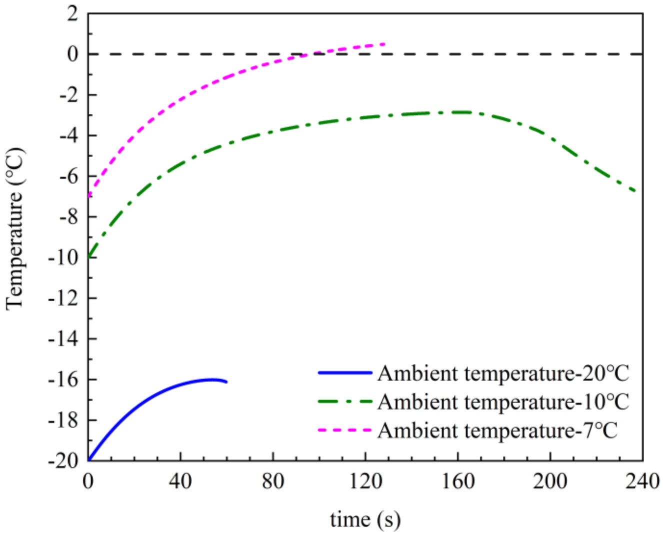

Fig. 6 Evolution of average temperature of PEMFC during the cold start processes of different initial temperatures

IV. EFFECT OF INTAKE HUMIDITY ON COLD START PERFORMANCE OF PEMFC

A. *Current Density During Cold Start Of PEMFC With Different Intake Humidity*

By modifying the boundary condition of the relative humidity of the cathode supply air, the effect of the inlet air's relative humidity on the sub-zero cold start performance of the PEMFC was analyzed. The study condition selected in this section simulates the low-temperature startup scenario of a single fuel cell with a PEM thickness of 0.127 mm at -10 °C, with the initial membrane water content in the cell set to 3.6 before startup. The relative humidity of the inlet air was set to 0%, 30%, and 60% for comparative study. The output current density curves of the cold start process under these three different inlet humidity conditions are shown in Figure 7.

As shown in the figure 7, the PEMFC cold start schemes with cathode inlet air relative humidity levels of 0%, 30%, and 60% all fail, as indicated by a rapid decrease in current density at approximately 250 seconds. The current density curves of the three schemes initially rise slowly and then decrease rapidly, which is consistent with the characteristics of a cold start. Although higher relative humidity results in slightly higher current density, the performance difference is minimal, with the maximum difference in current density being only 0.005 A·cm^{-2} at 230 seconds. In addition, towards the end of the cold start period at approximately 290 seconds, the output current density of the PEMFC with high inlet humidity begins to fall below that of the no inlet humidification scheme. This phenomenon may be attributed to the fact that internal ice accumulation becomes a dominant factor in the middle and late stages of the cold start process, during which the sensitivity to the concentration of internal water in the fuel cell increases. Comparing the cold start performance under three cathode inlet relative humidity conditions, it can be concluded that the impact of relative humidity variations on PEMFC output performance is not significant during cold starts at -10 °C.

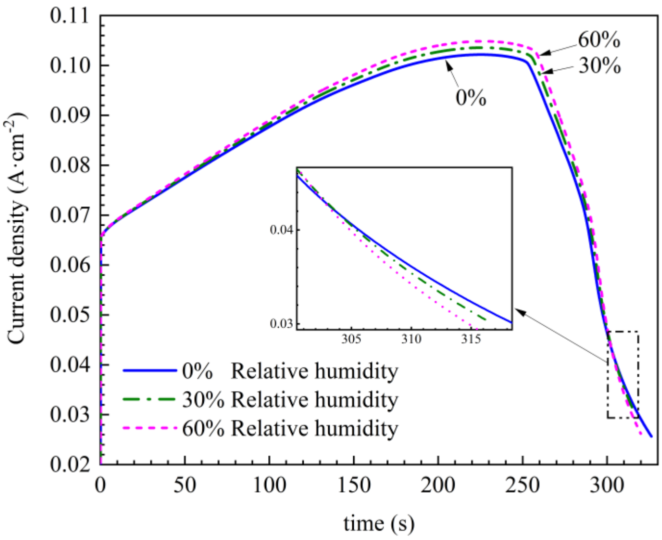

Fig. 7 Evolution of output current density of PEMFC during the cold start processes of different cathode inlet relative humidity

B. *Ice Volume Fraction During Cold Start Of PEMFC At Different Intake Humidity*

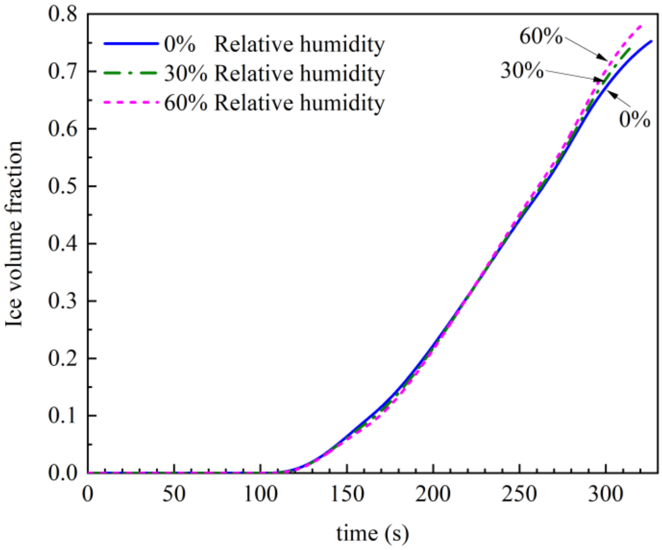

Fig. 8 Evolution of ice volume fraction in cathode CL during the cold start processes of different cathode inlet relative humidity

The cold start process was investigated for three different cathode inlet humidification levels in a -10 °C environment. Figure 8 shows that the cathode ice volume fractions for the three inlet humidification schemes remain essentially the consistent for most of the cold start process. However, towards the end phase of the cold start at approximately 290 seconds, the average ice volume fraction of the CCL for the high relative humidity intake scheme increases slightly, and the ice accumulation rate accelerates.

Figure 9 further reveals that the difference in the ice volume fraction in the CL at the end of the cold start is mainly concentrated near the inlet of the flow channel, with more severe ice accumulation in the inlet area under high inlet humidity. It was also observed that ice crystals tend to form first under the rib of the flow channel near the outlet side during the initial startup period and gradually spread across the entire CL over time. All schemes began to experience ice formation in the CCL approximately 110 seconds after startup. Subsequently, the accumulation of ice crystals led to a slowdown in the electrochemical reaction rate, and the reaction essentially ceased by 320 seconds, resulting in startup failure. These results further demonstrate that unassisted self-starting of the PEMFC is difficult to achieve at temperatures of -10 °C or lower.

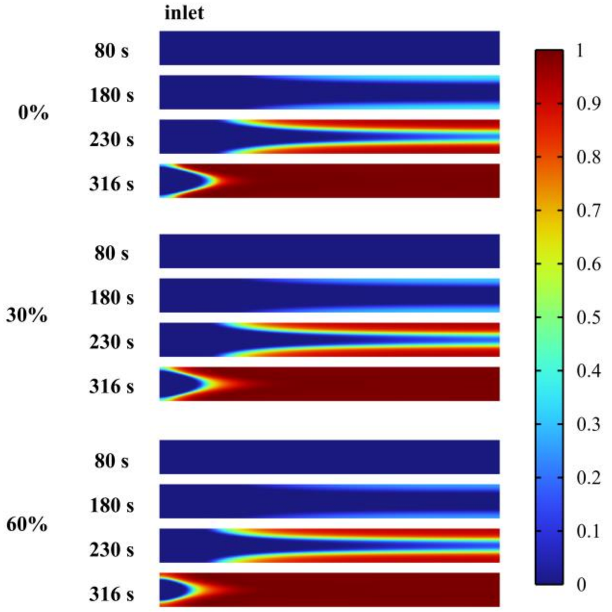

Fig. 9 Evolution of distribution of ice volume fraction in cathode CL during the cold start processes of different cathode inlet relative humidity

C. *Temperature Changes During Cold Start Of PEMFC At Different Intake Humidity*

Figure 10 below compares the average temperature changes of the PEMFC during the -10 °C cold start for three cathode inlet humidity levels. At the beginning of the startup, the average PEMFC temperature increases rapidly due to the electrochemical reaction, reaching its peak at approximately 260 seconds, with temperatures of -2.53 °C, -2.65 °C, and -2.77 °C, respectively. Higher inlet relative humidity ensures better hydration of ionomers in the membrane electrodes at the beginning of cold start, and higher proton conductivity helps enhance the electrochemical reaction rate in the PEMFC, thus outputting higher current density and generating more reaction heat to help the cell warming up, and thus the 60% relative humidity scenario is shown as having a higher average temperature during cold start in the graph. After reaching the highest point, the average cell temperature drops rapidly again. This is because the ice accumulation in the catalytic layer of the cathode of the fuel cell becomes more and more serious at the end of the cold start stage, and the electrochemical reaction in the porous electrodes is on the verge of stopping, and at this time, the temperature difference between the outer wall of the cell and the environment is large and there is a strong convective heat transfer between the outer wall and the sub-zero environment, so the temperature decreases rapidly, and this temperature curve proves that all the three cold start schemes have failed.

At -10 °C, the water saturation vapor pressure is low, and the difference in the relative humidity of the cathode inlet has no significant effect on the molar content of water in the supplied air. As a result, there is little difference in the outcomes of the three inlet humidity schemes. Ultimately, the current density of all three schemes drops sharply after 260 seconds, and the average fuel cell temperature decreased from approximately -3 °C to -6 °C, demonstrating unsuccessful self-start capability at this environmental temperature.

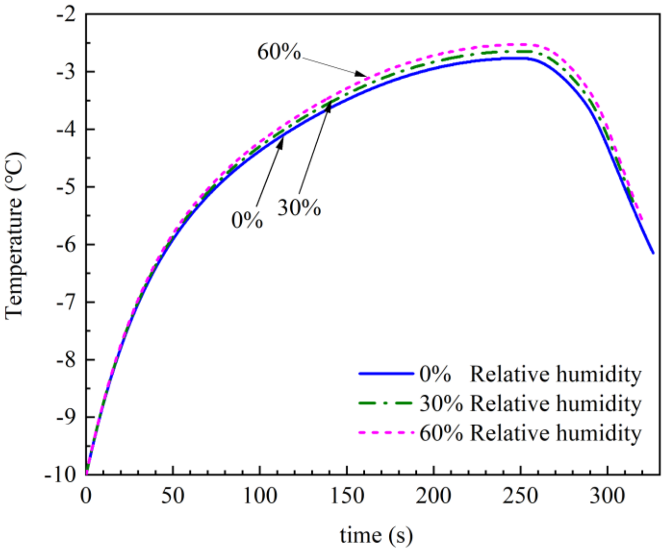

Fig. 10 Evolution of average temperature of PEMFC during the cold start processes of different cathode inlet relative humidity

V. CONCLUSION

In this paper, a transient three-dimensional numerical simulation of the PEMFC sub-zero ambient cold start process was conducted by modeling cold start conditions to investigate the effects of sub-zero ambient temperature and the relative humidity of the cathode supply air on cold start performance. The study results are as follows:

1) Ambient temperature is a critical factor determining the success or failure of PEMFC cold start. A higher ambient temperature promotes an increase in current density during the early stage of cold start, enhances electrochemical heat generation, improves the water storage capacity of the membrane electrode, delays ice formation, and increases the success rate of rapid self-start. It was also observed that a higher ambient temperature helps delay the moment of cold start failure.

2) Changes in the relative humidity of the cathode inlet air in sub-zero environment have a limited effect on cold start performance, this factor is not enough to change the outcome of a cold start. Although they can slightly increase current density in the initial and middle stages, they may exacerbate ice accumulation in the later stages, worsening performance and the average ice volume fraction in the catalytic layer is higher than that in the non-humidified air intake scheme. Therefore, when starting PEMFC in a sub-zero environment, it is recommended to use non-humidified inlet air to reduce the risk of ice formation.

3) The trend of ice distribution in the cathode catalyst layer during the cold start stage of the PEMFC is as follows: at the beginning of the startup period, ice tends to form under the rib of the flow channel near the outlet side. Over time, the ice crystals gradually grow and spread toward the inlet side, eventually occupying most of the porous electrode pore space. When the ice volume fraction reaches a critical value, a steep drop in current density along with a drop back in cell temperature means that the cold start is heading for failure.

REFERENCES

[1] X. Xie, G. Zhang, J. Zhou, *et al.*, "Experimental and theoretical analysis of ionomer/carbon ratio effect on PEM fuel cell cold start operation," *Int. J. Hydrogen Energy*, vol. 42, no. 17, pp. 12521–12530, 2017.

[2] S. T. Cui, D. L. Wang, X. Q. Yan, *et al.*, "Study on low temperature unassisted start-up of fuel cell stack (in Chinese)," *Chin. J. Power Sources*, vol. 44, pp. 1451–1455, 2020.

[3] D. Zhong, R. Lin, L. Han, *et al.*, "Mechanism analysis of the effect of different gas manifold positions on proton exchange membrane fuel cell cold start performance," *Int. J. Energy Res.*, vol. 45, no. 9, pp. 13429–13441, 2021.

[4] H. Min, Q. Cao, Y. Yu, *et al.*, "A cold start mode of proton exchange membrane fuel cell based on current control," *Int. J. Hydrogen Energy*, vol. 47, no. 8, pp. 5507–5520, 2022.

[5] A. D. Santamaria, J. Bachman, and J. W. Park, "Cold-start of parallel and interdigitated flow-field polymer electrolyte membrane fuel cell," *Electrochim. Acta*, vol. 107, pp. 327–338, 2013.

[6] Y. Luo, Q. Guo, *et al.*, "Analysis of cold start processes in proton exchange membrane fuel cell stacks," *J. Power Sources*, vol. 224, pp. 99–114, 2013.

[7] R. J. Balliet and J. Newman, "Cold start of a polymer-electrolyte fuel cell I. Development of a two-dimensional model," *J. Electrochem. Soc.*, vol. 158, no. 8, pp. B927–B938, 2011.

[8] L. Yang, C. Cao, Q. Gan, *et al.*, "Revealing failure modes and effect of catalyst layer properties for PEM fuel cell cold start using an agglomerate model," *Appl. Energy*, vol. 312, p. 118792, 2022.

[9] L. Zang, L. Hao, and X. Zhu, "Effect of the pore structure of cathode catalyst layer on the PEM fuel cell cold start process," *Energy*, vol. 271, p. 126993, 2023.

[10] F. Jiang, C. Y. Wang, and K. S. Chen, "Current ramping: A strategy for rapid start-up of PEMFCs from subfreezing environment," *J. Electrochem. Soc.*, vol. 157, no. 3, pp. 342–347, 2010.

[11] E. Pinton, Y. Fourneron, S. Rosini, *et al.*, "Experimental and theoretical investigations on a proton exchange membrane fuel cell starting up at subzero temperatures," *J. Power Sources*, vol. 186, pp. 80–88, 2009.

[12] J. Tao, X. Wei, and H. Dai, "Study on the constant voltage, current and current ramping cold start modes of proton exchange membrane fuel cell," in *Proc. SAE WCX Digit. Summit*, Warrendale, PA, USA: SAE Int., 2021, Art. no. 2021-01-0746.

[13] K. Jiao and X. Li, "Three-dimensional multiphase modeling of cold start processes in polymer electrolyte membrane fuel cells," *Electrochim. Acta*, vol. 54, no. 27, pp. 6876–6891, 2009.

[14] K. Jiao and X. Li, "Effects of various operating and initial conditions on cold start performance of polymer electrolyte membrane fuel cells," *Int. J. Hydrogen Energy*, vol. 34, no. 19, pp. 8171–8184, 2009.